acta physica slovaca vol. 47 No. 1, 95 – 106 February 1997

HANBURY-BROWN/TWISS INTERFEROMETRY BEYOND THE GAUSSIAN APPROXIMATION[1]

Urs Achim Wiedemann[2] **Ulrich Heinz**
Institut für Theoretische Physik, Universität Regensburg
D-93040 Regensburg, F R Germany

Received 29 October 1996, accepted 13 January 1997

We review recent results on resonance decay contributions to 2-particle Hanbury-Brown/Twiss correlation functions $C(\mathbf{q},\mathbf{K})$. Due to the resonance decays, the correlator $C(\mathbf{q},\mathbf{K})$ shows deviations from a Gaussian shape. Hence, the spatio-temporal information contained in the correlator can be extracted only partly from its Gaussian fit parameters. To extract more information, higher order q-moments provide an appropriate tool. At least in the models with resonance decays studied so far, these additional observables provide the cleanest distinction between scenarios with and without transverse flow.

1. Introduction

Two-particle correlations of identical particles are the only known observables which give access to the spatio-temporal evolution of heavy ion collisions. According to the main result of the coherent state formalism [1], they are determined by the Fourier transform of the emission function $S(x,K) = \frac{1}{2}(p_1+p_2)$ with respect to the relative pair momentum $q = p_1 - p_2$, [1, 2, 3, 4, 5]

$$C(\mathbf{q},\mathbf{K}) = 1 + \frac{\left|\int d^4x\, S(x,K)\, e^{iq\cdot x}\right|^2}{\left|\int d^4x\, S(x,K)\right|^2}. \tag{1}$$

Here, the emission function $S(x,p)$ has an interpretation as Wigner phase space density. It describes the probability that a particle of momentum p is emitted from a space-time point x.

The aim of HBT interferometry is to extract via the measurement of $C(\mathbf{q},\mathbf{K})$ as much information as possible about the spatio-temporal distribution $S(x,K)$. So far, the interplay between the experimentally measurable momentum correlator $C(\mathbf{q},\mathbf{K})$ and the theoretical concept of the space-time emission function $S(x,K)$ was investigated mainly

[1] Presented at the Heavy Ion Workshop on Particle Physics, Sept. 2.-6, 1996, Bratislava, Slovakia
[2] E-mail address: Urs.Wiedemann@physik.uni-regensburg.de

in the context of Gaussian approximations for both [3, 6, 5, 7, 8]. However, resonance decay contributions can lead to deviations of $C(\mathbf{q},\mathbf{K})$ from a Gaussian shape [9, 10]. In this lecture, we review recent results [11] of how resonance contributions influence HBT correlation functions and we explain how one can quantify systematically and exploit subsequently the non-Gaussian features of the correlator.

2. HBT interferometry in the Gaussian framework

We start by shortly reviewing the (cartesian) Gaussian parametrization of the correlation function for an azimuthally symmetric emissions function (i.e., $S(x,K)$ is invariant under $y \to -y$), [5]

$$C(\mathbf{K},\mathbf{q}) = 1 + \lambda\, e^{-R_o^2(\mathbf{K})q_o^2 - R_s^2(\mathbf{K})q_s^2 - R_l^2(\mathbf{K})q_l^2 - 2R_{ol}^2(\mathbf{K})q_o q_l}\,. \tag{2}$$

Here, the relative momentum components are chosen parallel to the beam (l = *longitudinal*), parallel to the transverse component of $\mathbf{K}$, (o = *out*) and in the remaining third direction (s = *side*).

Since the Gaussian fit parameters $R_{ij}^2(\mathbf{K})$ allow to extract only "Gaussian" information about the space-time emission function, they can be extracted from a Gaussian ansatz for the emission function $S(x,K)$ in terms of space-time variances $(B^{-1})_{\mu\nu}$, [14, 8]

$$\begin{aligned} S(x,K) &\simeq S(\bar{x},K)\, e^{-\frac{1}{2}\tilde{x}^\mu \tilde{x}^\nu B_{\mu\nu}(\mathbf{K})}\,, \\ (B^{-1})_{\mu\nu} &= \langle x_\mu x_\nu\rangle - \langle x_\mu\rangle\langle x_\nu\rangle = \langle \tilde{x}_\mu \tilde{x}_\nu\rangle\,, \\ \langle \xi\rangle &= \langle \xi\rangle(K) = \frac{\int d^4x\, \xi\, S(x,K)}{\int d^4x\, S(x,K)}\,, \end{aligned} \tag{3}$$

where $\tilde{x}_\mu = x_\mu - \langle x_\mu\rangle$ denotes space-time variables shifted by $\bar{x} = \bar{x}(\mathbf{K}) = \langle x_\mu\rangle$. Inserting (3) back into (1), one finds

$$C(\mathbf{K},\mathbf{q}) = 1 + e^{-(B^{-1})_{\mu\nu}q^\mu q^\nu}\,. \tag{4}$$

Due to the mass-shell condition of the detected particles, only three of the four relative momentum components of this equation are independent, the fourth is given via the on-shell constraint $q^0 = \frac{\mathbf{K}}{K_0}\cdot \mathbf{q} = \beta\cdot\mathbf{q}$. This constraint implies that the Fourier transform in (1) does not have a unique inverse.

The HBT-radii in (2) are commonly derived by inserting the on-shell constraint into (4) and reading off the linear combinations of the $(B^{-1})_{\mu\nu}$, [14, 8], or via the second derivatives of (1) [5]

$$\begin{aligned} R_{ij}^2(\mathbf{K}) &= \langle (x_i - \beta_i t)(x_j - \beta_j t)\rangle - \langle (x_i - \beta_i t)\rangle\langle (x_j - \beta_j t)\rangle\,, \\ &= -\left.\frac{d^2\, C(\mathbf{q},\mathbf{K})}{dq_i\, dq_j}\right|_{\mathbf{q}=0}\,. \end{aligned} \tag{5}$$

Hence, the expressions $R_{ij}(\mathbf{K})$ denote the curvature components of the correlator $C(\mathbf{q},\mathbf{K})$ at $\mathbf{q}=0$ and coincide with the half widths of the correlator only if the correlator is sufficiently Gaussian.

Depending on how the on-shell constraint $q^0 = \beta\cdot\mathbf{q}$ is resolved in (4), different Gaussian parametrizations can be obtained. Especially, using q^0, $q_\perp = \sqrt{q_o^2+q_s^2}$ and q_l as independent relative momentum components, one is lead to the Yano-Koonin-Podgoretskii parametrization [12, 13, 14, 15, 16]

$$C(\mathbf{K},\mathbf{q}) = 1 + \lambda\, e^{-R_\perp^2(\mathbf{K})\, q_\perp^2 - R_\parallel^2(\mathbf{K})(q_l^2 - (q^0)^2) - (R_0^2(\mathbf{K}) + R_\parallel^2(\mathbf{K}))(q\cdot U(\mathbf{K}))^2}\,, \tag{6}$$

where $U(\mathbf{K}) = \gamma(\mathbf{K})\,(1,0,0,v(\mathbf{K}))$, $\gamma = \frac{1}{\sqrt{1-v^2}}$ is a (K-dependent) 4-velocity with only a longitudinal spatial component. This parametrization has the advantage that the YKP parameters $R_\perp^2(\mathbf{K})$, $R_0^2(\mathbf{K})$, and $R_\parallel^2(\mathbf{K})$ extracted from such a fit do not depend on the longitudinal velocity of the observer system in which the correlation function is measured. Their physical interpretation is easiest in terms of coordinates measured in the frame where $v(\mathbf{K})$ vanishes. There they are given in the Gaussian framework by [14, 15]

$$R_\perp^2(\mathbf{K}) = \langle \tilde{y}^2\rangle, \quad R_\parallel^2(\mathbf{K}) \approx \langle \tilde{z}^2\rangle\,, \quad R_0^2(\mathbf{K}) \approx \langle \tilde{t}^2\rangle\,. \tag{7}$$

For a detailed discussion of the physical meaning of the YKP parameters see Refs. [15, 16].

The main importance of the above expressions (5,7) for the HBT parameters resides in providing an intuitive understanding of which space-time features of the source are reflected by the various q-dependencies of the correlator.

3. Resonance Decay Contributions to HBT Correlation Radii

3.1. A model including resonance decays

A model is specified by a particular choice of a pion emission function. In the presence of resonance decays, the emission function is the sum of a direct term plus one additional term for each contributing decay channel of each resonance species,

$$S_\pi(x,p) = S_\pi^{\rm dir}(x,p) + \sum_R S_{R\to\pi}(x,p)\,. \tag{8}$$

We have used for our analysis a simple analytical model which assumes local thermalization at freeze-out and produces hadronic resonances by thermal excitation. The emission function for particle species i is taken as

$$\begin{aligned} S_i^{\rm dir}(x,P) &= \frac{2J_i+1}{(2\pi)^3}\, P\cdot n(x)\, \exp\left(-\frac{P\cdot u(x) - \mu_i}{T}\right) H(x) \\ H(x) &= \sqrt{\frac{2}{\pi}}\, \frac{1}{\sqrt{2\pi(\Delta\eta)^2}}\, \exp\left(-\frac{r^2}{2R^2} - \frac{\eta^2}{2(\Delta\eta)^2} - \frac{(\tau-\tau_0)^2}{2(\Delta\tau)^2}\right)\,. \end{aligned} \tag{9}$$

Here, the factor $2J_i + 1$ counts the spin degeneracy, and the Boltzmann factor $\exp[-(P\cdot u(x) - \mu_i)/T]$ implements both the assumption of thermalization, with temperature T and chemical potential μ_i, and collective expansion with hydrodynamic flow 4-velocity $u_\mu(x)$. Space-time is parametrized via longitudinal proper time $\tau = \sqrt{t^2 - z^2}$, space-time rapidity $\eta = \frac{1}{2}\ln[(t+z)/(t-z)]$, transverse radius r and azimuthal angle ϕ, with volume element $d^4x = \tau\, d\tau\, d\eta\, r\, dr\, d\phi$. The gaussian factors $\exp[-r^2/(2R^2)]$ and $\exp[-\eta^2/(2(\Delta\eta)^2)]$ specify the geometric extensions of the source. Freeze-out is characterized by hypersurfaces $\Sigma_\tau(x) = (\tau\cosh\eta, r\cos\phi, r\sin\phi, \tau\sinh\eta)$ of constant longitudinal proper time τ, with normal vector $n^\mu(x)$, with the last factor in (9) providing a gaussian average over proper time around the mean value τ_0 with dispersion $\Delta\tau$. With these assumptions the flux factor $P\cdot n(x)$ in (9) reduces to $P\cdot n(x) = M_\perp \cosh(Y-\eta)$.

We choose an expansion flow profile

$$u^\mu(x) = (\cosh\eta_l \cosh\eta_t, \sinh\eta_t\cos\phi, \sinh\eta_t\sin\phi, \sinh\eta_l\cosh\eta_t)\,, \qquad \eta_t(r) = \eta_f\left(\frac{r}{R}\right), \tag{10}$$

where the longitudinal flow velocity v_l is assumed to satisfy Bjorken scaling [17], $v_l = z/t$, i.e. we identify the longitudinal flow rapidity $\eta_l = \frac{1}{2}\ln[(1+v_l)/(1-v_l)]$ with the space-time rapidity η. The transverse expansion flow η_t is a linear function of r.

From the direct emission function $S_R^{\rm dir}(X,P)$ for the resonance decay channel R, given in (9), we calculate the pion contribution $S_{R\to\pi}(x,p)$ as

$$S_{R\to\pi}(x;p) = M\int_{s_-}^{s_+} ds\, g(s) \int \frac{d^3P}{E_P}\delta(P\cdot p - ME^*)\int d^4X \times \int d\tau\, \Gamma e^{-\Gamma\tau}\delta^{(4)}\left(x - \left(X + \frac{P}{M}\tau\right)\right) S_R^{\rm dir}(X,P). \tag{11}$$

Here, capital letters denote variables associated with the parent resonance, while lower case letters denote pion variables. Variables with a star denote their values in the resonance rest frame, all other variables are given in the fixed measurement frame.

According to (11), a resonance R, emitted with momentum P from a space-time point X^μ, decays after a proper time τ at $x^\mu = X^\mu + \frac{P^\mu}{M}\tau$ into a pion of momentum p and $(n-1)$ other decay products, $R \longrightarrow \pi + c_2 + c_3 + \ldots + c_n$. The decay rate at proper time τ is $\Gamma e^{-\Gamma\tau}$ where Γ is the total decay width of R. Here $s = (\sum_{i=2}^n p_i^*)^2$ is the squared invariant mass of the $(n-1)$ unobserved decay products. It can vary between $s_- = (\sum_{i=2}^n m_i)^2$ and $s_+ = (M-m)^2$. $g(s)$ is the decay phase space for these particles stemming from an unpolarized resonance with isotropic decay in its rest frame. The δ-function $\delta(P\cdot p - ME^*)$ implements the energy momentum constraint on the resonance decay, E^* being the energy of the observed decay pion in the resonance rest frame.

3.2. Results for the correlator

For the model specified by (8-11), we have calculated numerically the 2-particle correlation function (1). All numerical calculations discussed here were done with the set

of source parameters $T = 150$ MeV, $R = 5$ fm, $\Delta\eta = 1.2$, $\tau_0 = 5$ fm/c, $\Delta\tau = 1$ fm/c and $\mu_B = \mu_S = 0$. Our study includes resonance decay channels of the resonances ρ, Δ, K^*, Σ^*, ω, η, η', K_S^0 and Σ. Calculating $C(\mathbf{q},\mathbf{K})$ for the direct emission function $S_\pi^{dir}(x,K)$ firstly and adding then resonance contributions R, we have studied the influence of resonance decays on the shape of the correlator, cf. Fig. 1. Here, we shortly discuss the main three effects (for more details, see Ref. [11]):

- the "lifetime effect"
  Due to their finite lifetime, resonances can propagate outside of the thermally equilibrated region before decaying. This tends to decrease the widths of the correlator. If R is relatively shortlived ($\Gamma > 36$ MeV, say), then the decay of R takes place close to its production point and the effect on the width of $C(\mathbf{q},\mathbf{K})$ is small. On the other hand, very longlived resonances ($\Gamma \ll 1$ MeV) propagate up to several *cm* which one cannot resolve on a MeV scale. Thus, they effectively contribute to the normalization of (1) only, thereby decreasing the intercept parameter λ. The ω-resonance finally with $\Gamma = 8.43$ MeV lies in between these extremes. It contributes significant "exponential tails" to the emission function and seriously distorts the Gaussian shape of the correlator.
- the "shrinking transverse size effect"
  In the presence of transverse flow, the transverse size R_t of the effective emission function S_R^{dir} of parent resonances shrinks for the model (9). In lowest order Gaussian approximation, it is

$$R_t = R\left(1 + \frac{M_\perp}{T}\eta_f^2\right)^{-\frac{1}{2}}, \tag{12}$$

which is smaller for resonances than for thermal pions. Accordingly, the shrinking transverse size effect tends to decrease the HBT radius parameters, i.e., it tends to counterbalance the lifetime effect.

- the "non-gaussisity" of the correlator
  Resonance decays contribute exponential tails to the emission function which result in a non-Gaussian q-dependence of the correlator. This follows form the Fourier transform of the emission function (11),

$$\int d^4x\, e^{iq\cdot x} S_{R\to\pi}(x,p) = \sum_\pm \int_R \frac{1}{1 - \frac{q\cdot P\pm}{M\Gamma}} \int d^4x\, e^{iq\cdot x} S_R^{dir}(x, P^\pm). \tag{13}$$

Here, $\int_R$ denotes the integral over the phase space of the parent resonances and $\sum_\pm$ sums over the two direction in which the resonance can propagate if the decay pion was emitted in the out-direction. The non-Gaussian term $\frac{1}{1-\frac{q\cdot P\pm}{M\Gamma}}$ stems from the exponential decay law and is most important for the ω-decay contribution. For shortlived resonances (Γ large), it is sufficiently close to unity, for very longlived resonances ($\Gamma \ll 1$ MeV) it dominates the q-dependence on a KeV-scale thereby affecting the normalization (i.e., the intercept parameter), but not the shape of the correlator (1).

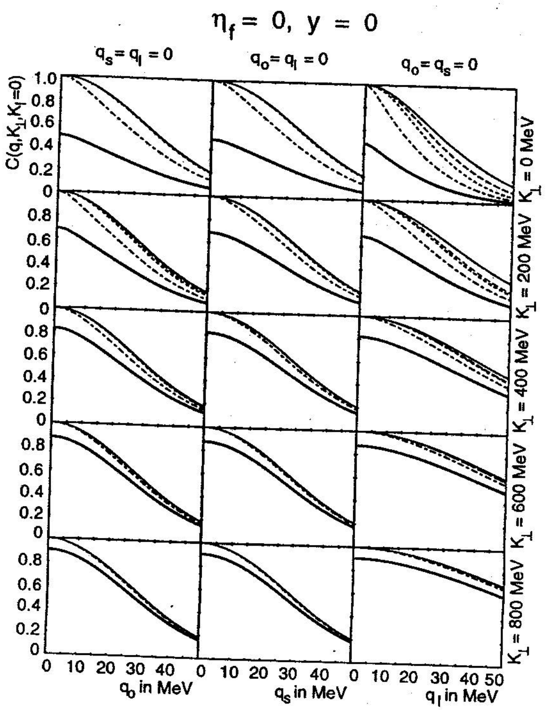

Fig. 1. Two-particle correlator $C(\mathbf{q}, \mathbf{K})$ for π^- pairs as a function of the different components of the relative momentum $\mathbf{q}$ and for different values of the transverse pair momentum $K_\perp$ and longitudinal pair rapidity $y = 0$. The lines denote calculations of the correlator for thermal pions only (straight lines), including ρ-decays (dashed lines), (ρ, Δ, Σ^* and K^*)-decays (dotted lines), (ρ, Δ, Σ^*, K^* and ω)-decays (dash-dotted lines), and all resonance contributions, including the longlived η, η', K_S^0 and Σ (thick straight lines).

4. Q-variances: HBT interferometry beyond the Gaussian approximation

For the spatio-temporal interpretation of the correlator, relatively small changes in the shape and K-dependence of the correlator are important. This makes it indispensable to describe the key features of $C(\mathbf{q}, \mathbf{K})$ with a small number of fit parameters. To this aim, the *Gaussian* HBT fit parameters $R^2_{ij}(\mathbf{K})$ are commonly used so far.

4.1. HBT radius parameters for non-Gaussian correlators

For non-Gaussian correlators, a definition of HBT radius parameters is required which does not presuppose a particular shape of $C(\mathbf{q}, \mathbf{K})$. Such a definition is provided by the second q-moments of the correlator

$$\langle\langle q_i\, q_j \rangle\rangle \equiv \frac{\int d^3\mathbf{q}\, q_i\, q_j\, [C(\mathbf{q},\mathbf{K}) - 1]}{\int d^3\mathbf{q}\, [C(\mathbf{q},\mathbf{K}) - 1]} = \frac{1}{2} \left(D^{-1}(\mathbf{K})\right)_{ij}, \tag{14}$$

and the corresponding intercept parameter

$$\lambda(\mathbf{K}) = \frac{\sqrt{\det D}}{\pi^{\frac{3}{2}}} \int d^3\mathbf{q}\, [C(\mathbf{q},\mathbf{K}) - 1]. \tag{15}$$

In contrast to a Gaussian ansatz, these expressions are well-defined for arbitrary shapes of the correlator $C(\mathbf{q}, \mathbf{K})$. For the special Gaussian case, where the correlator is given in terms of three independent relative momentum components q_i,

$$C(\mathbf{q},\mathbf{K}) = 1 + \lambda\, e^{-q_i\, D_{ij}(\mathbf{K})\, q_j}, \tag{16}$$

the second q-moments are directly related to the Gaussian fit parameters. Especially, one finds for the cartesian parametrization (2)

$$D_{ij}(\mathbf{K}) = \begin{pmatrix} R_o^2 & 0 & R_{ol}^2 \\ 0 & R_s^2 & 0 \\ R_{ol}^2 & 0 & R_l^2 \end{pmatrix} \qquad i,j = o,s,l\,. \tag{17}$$

For the YKP parametrization (6), the corresponding expression reads

$$D_{ij}(\mathbf{K}) = \begin{pmatrix} R_{00}^2 & 0 & R_{03}^2 \\ 0 & R_\perp^2 & 0 \\ R_{03}^2 & 0 & R_{33}^2 \end{pmatrix} \qquad i,j = 0,\perp,l\,, \tag{18}$$

where the YKP parameters v, R_0 and $R_\parallel$ are determined from R_{00}, R_{03} and R_{33},

$$\begin{aligned} v &= \frac{-1}{2D}\left(1 - \sqrt{1 - (4D^2)^2}\right), \qquad D = \frac{R_{03}^2}{R_{00}^2 + R_{33}^2}, \\ R_0^2 &= \frac{R_{00}^2 - v^2\, R_{33}^2}{1 + v^2}, \\ R_\parallel^2 &= \frac{R_{33}^2 - v^2\, R_{00}^2}{1 + v^2}. \end{aligned} \tag{19}$$

For $D = 0$, one has $v = 0$, $R_{00} = R_0$ and $R_\parallel = R_{33}$.

4.2. Beyond the Gaussian approximation: 1-dimensional q-variances

For a correlator of Gaussian shape, the definitions (14) for the second q-moments and (19) for the intercept parameter coincide with the results of a Gaussian fit. Their advantage is firstly that they are well-defined for non-Gaussian correlators, too. Secondly, they can be used to study systematically deviations of the correlator from a Gaussian shape. Here, we illustrate this point for 1-dimensional q-variances whose second q-moments are given by

$$\langle\langle q_i^2 \rangle\rangle = \frac{\int dq_i\, q_i^2\, [C(q_i, q_{i\neq j} = 0, \mathbf{K}) - 1]}{\int dq_i\, [C(q_i, q_{i\neq j} = 0, \mathbf{K}) - 1]}, \tag{20}$$

$$\langle\langle q_i^2 \rangle\rangle = \frac{1}{2R_i^2} \quad \text{for the Gaussian correlator (23)}, \tag{21}$$

$$\lambda_i(\mathbf{K}) = \frac{R_i}{\sqrt{\pi}} \int dq_i\, [C(q_i, q_{i\neq j} = 0, \mathbf{K}) - 1]. \tag{22}$$

These provide for a correlator of arbitrary shape the information corresponding to the Gaussian fit

$$C(q_i, q_{i\neq j} = 0, \mathbf{K}) = 1 + \lambda_i e^{-R_i^2 q_i^2}. \tag{23}$$

The key to quantitative statements about non-Gaussian features of $C(\mathbf{q}, \mathbf{K})$ are the higher q-moments

$$\langle\langle q_i^n \rangle\rangle = \frac{\int dq_i\, q_i^n\, [C(q_i, q_{i\neq j} = 0, \mathbf{K}) - 1]}{\int dq_i\, [C(q_i, q_{i\neq j} = 0, \mathbf{K}) - 1]}, \tag{24}$$

$$\langle\langle q_i^{2m} \rangle\rangle = \frac{(2m-1)!!}{(2R_i^2)^m} \quad \text{for the Gaussian correlator (23)}, \tag{25}$$

$$\langle\langle q_i^{2m+1} \rangle\rangle = 0 \quad \text{for reflection symmetric correlators}. \tag{26}$$

In general, higher q-moments contain combinatorial factors of the "Gaussian" second moments $\langle\langle q_i^2 \rangle\rangle$ (cf. (25)), as well as non-Gaussian information. The interesting quantities are therefore the cumulants which remove the trivial Gaussian contributions to the higher order moments by subtraction:

$$\Delta_i^{(2m)} = \frac{1}{(2m-1)!!} \frac{\langle\langle q_i^{2m} \rangle\rangle}{\langle\langle q_i^2 \rangle\rangle^m} - 1. \tag{27}$$

The normalization removes the dependence on the Gaussian widths of $C(\mathbf{q}, \mathbf{K})$ and provides a dimensionless measures for deviations from a Gaussian shape. Here, we restrict our discussion of non-Gaussian features to the "kurtosis"

$$\Delta_i = \frac{\langle\langle q_i^4 \rangle\rangle}{3\, \langle\langle q_i^2 \rangle\rangle^2} - 1. \tag{28}$$

4.3. Results for q-moments

For the model (9) of an emission function including resonance decays, we have determined the 1-dimensional second moments (20) and the kurtosis (28). Here, we shortly summarize the main results (for more details, see Ref. [11]):

- Second q-moments contain unbiased "Gaussian information".
  In our model studies, the inverse second q-moments $\frac{1}{\langle\langle q_i^2 \rangle\rangle}$ coincide with the Gaussian fit parameters R_i extracted for a set of n equidistant points $q_i^{(j)}$ between 0 and 50 MeV from

$$\sum_{j=1}^{n} \left(\log C(q_i^{(j)}, q_{i' \neq i} = 0, \mathbf{K}) - \log \lambda + R_i^2 q_i^{(j)^2}) \right)^2 = \min. \tag{29}$$

  If the fit (29) is applied to a different intervall, between 0 and 250 MeV, say, then the HBT fit parameter R_i in (29) change due to the non-Gaussian shape of the correlator. In contrast, the second q-moments do not depend on such additional specifications of the extraction procedure.

- Resonance decay contributions to the HBT-radii $R_i^{q_i}$, cf. Fig. 2.
  Due to the lifetime effect, resonances (most prominently the ω) lead to an increase of R_s especially in the low $K_\perp$-regime where their relative abundance is high. This induces for vanishing transverse flow $\eta_f = 0$ a finite slope. For finite transverse flow $\eta_f = 0.3$, the side radius remains virtually unaffected. The reason is that here, the "shrinking transverse size effect" counterbalances the lifetime effect.
  The out radius R_o receives contributions from both the x- and t-dependence of the emission function. Due to resonance decays, the effective emission duration of $S(x, K)$ increases significantly and this induces an enhanced increase of R_o on a scale proportional to $\beta_\perp$. In the presence of transverse flow, this is partly compensated by the shrinking transverse size effect.
  For the longitudinal radius finally, resonance decay contributions result in a significant increase of R_l in the low $K_\perp$-region.

- Deviations of C from a Gaussian shape, cf. Fig. 2.
  In the model (9), the exponential tails due to resonance contributions affect the correlator for vanishing transverse flow more significantly. At finite transverse flow, S_π^{dir} is spatially more extended in the transverse direction than S_R^{dir} and "covers" a substantial part of the exponential tails of $S_{R\to\pi}$. Hence, the total emission function (8) and a fortiori the correlator deviate for finite transverse flow less from a Gaussian shape and quantitative statements about non-Gaussian features of $C(\mathbf{K})$ allow to distinguish between scenarios with and without transverse flow. As seen in Fig. 2. , Δ_s provides the cleanest signal for this distinction. Furthermore, we note that Δ_o shows an increase proportional to $\beta_\perp$. This can be traced back to the non-Gaussian features of $S(x, K)$ which are particularly prominent in its t-dependence.

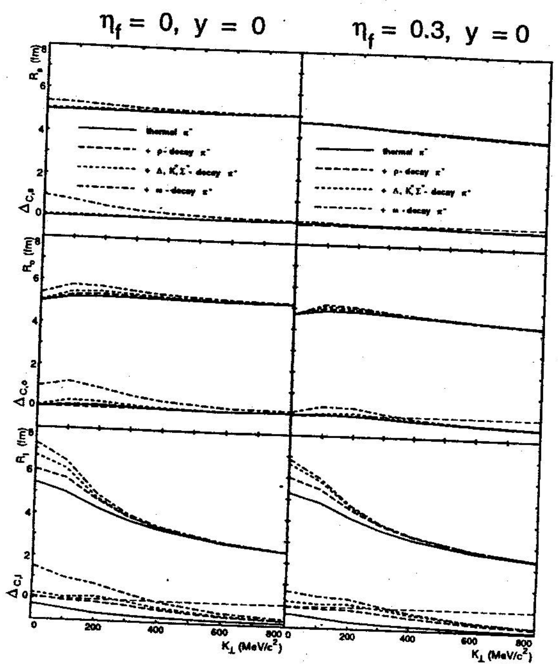

Fig. 2. The inverted second q-moments R_i according to (20), and the corresponding truncated fourth q-moments Δ_i which characterize the deviation of $C(\mathbf{q},\mathbf{K})$ from a Gaussian shape. These deviations provide the cleanest signal to distinguish the scenarios without ($\eta_f = 0$) and with ($\eta_f = 0.3$) transverse flow.

The non-Gaussian features in the longitudinal direction are significant already for the thermal contributions. They can be traced back to the $\cosh(\eta - y)$ terms in the Boltzmann factor of (9) which lead to a non-Gaussian η-dependence of the thermal emission function, cf. [8].

5. Concluding remarks

Over the past years, the experimental data for 2-particle pion correlations in ultra-relativistic heavy ion collisions have improved tremendously. They are now becoming

sufficiently accurate to extract not only the Gaussian widths of the correlator but also its finer structures. Here, we have shown that q-variances provide an appropriate tool for the quantitative discussion of non-Gaussian deviations of C and we have seen that higher order q-moments allow to distinguish between physical scenarios which are difficult to resolve on the basis of Gaussian fit parameters. Especially, in the models studied so far, the kurtosis Δ_s provides the cleanest signal for transverse flow.

As an additional advertisement for q-variances, we sketch here how q-variances can be calculated directly from the emission function via model-independent expressions. The starting point is the generating functional

$$Z(\mathbf{y},\mathbf{K}) = \int d^3q\, e^{i\mathbf{q}\cdot\mathbf{y}}\, [C(\mathbf{q},\mathbf{K}) - 1]\,, \tag{30}$$

whose derivatives define both second and higher order q-moments,

$$\langle\!\langle q_{i_1}\, q_{i_2} ... q_{i_n} \rangle\!\rangle = (-i)^n \frac{\partial^n}{\partial y_{i_1} \partial y_{i_2} ... \partial y_{i_n}} \ln Z(\mathbf{y},\mathbf{K}) \Big|_{\mathbf{y}=0}\,. \tag{31}$$

From this generating function, the correlator can be reconstructed completely. The series of n-th q-variances (31) is merely a convenient way to characterize its shape starting with its "Gaussian" widths $\langle\!\langle q_i q_j \rangle\!\rangle$ and going for increasing n step by step to finer structures.

To calculate $Z(\mathbf{y},\mathbf{K})$ directly from a given emission function it is convenient to use the normalized "relative distance distribution"

$$\rho(u;K) = \int d^4X\, s(X + \tfrac{u}{2}, K)\, s(X - \tfrac{u}{2}, K)\,, \tag{32}$$

$\int d^4u\, \rho(u;K) = 1$, written in terms of the normalized emission function $s(x,K) = S(x,K)/\int d^4x\, S(x,K)$. ρ is real and even in u. Then

$$Z(\mathbf{y},\mathbf{K}) = \int d^3q\, e^{i\mathbf{q}\cdot\mathbf{y}} \int d^4u\, e^{iq\cdot u}\, \rho(u;K)\,. \tag{33}$$

In the Cartesian parametrization, this expression reduces to a one-dimensional integral

$$Z(\mathbf{y},\mathbf{K}) = \int dt\, \rho(y_s, y_o + \beta_\perp t, y_l + \beta_l t, t; K)\,. \tag{34}$$

which can simplify model studies considerably. A similar formalism can be used for 1-dimensional q-variances, [11].

Acknowledgements This report is based on joint work [11], and was supported by BMBF, DFG and GSI. One of us (U.A.W.) would like to thank Prof. S. Kumar for kind hospitality at Yale University where this report was written.

References

[1] M. Gyulassy, S.K. Kauffmann, L.W. Wilson: *Phys. Rev. C* **20**, 2267 (1979).
[2] E. Shuryak: *Phys. Lett. B* **44**, 387 (1973); *Sov. J. Nucl. Phys.* **18**, 667 (1974).
[3] S. Pratt, T. Csörgő, J. Zimányi: *Phys. Rev. C* **42**, 2646 (1990).
[4] S. Chapman, U. Heinz: *Phys. Lett. B* **340**, 250 (1994).
[5] S. Chapman, P. Scotto, U. Heinz: *Phys. Rev. Lett.* **74**, 4400 (1995).
[6] T. Csörgő, B. Lørstad, J. Zimányi: *Z. Phys. C* **71**, 491 (1996).
[7] M. Herrmann, G.F.Bertsch: *Phys. Rev. C* **51**, 328 (1995).
[8] U.A. Wiedemann, P. Scotto, U. Heinz: *Phys. Rev. C* **53**, 918 (1996).
[9] B.R. Schlei, U. Ornik, M. Plümer, R. M. Weiner: *Phys. Lett. B* **293**, 275 (1992); J. Bolz, U. Ornik, M. Plümer, B.R. Schlei, R. M. Weiner: *Phys. Lett. B* **300**, 404 (1993); *Phys. Rev. D* **47**, 3860 (1993).
[10] H. Heiselberg: *Phys. Lett. B* **379**, 27 (1996).
[11] U.A. Wiedemann, U. Heinz: Los Alamos eprint archive nucl-th/9611031.
[12] F. Yano, S. Koonin: *Phys. Lett. B* **78**, 556 (178).
[13] M.I. Podgoretsky: *Sov. J. Nucl. Phys.* **37**, 272 (1983).
[14] S. Chapman, J.R. Nix, U. Heinz: *Phys. Rev. C* **52**, 2694 (1995).
[15] U. Heinz, B. Tomášik, U.A. Wiedemann, Wu Y.-F.: *Phys. Lett. B* **382**, 181 (1996).
[16] Wu Y.-F., U. Heinz, B. Tomášik, U.A. Wiedemann: Los Alamos eprint archive nucl-th/9607044.
[17] J.D. Bjorken: sl Phys. Rev. D **27** (1983), 140.